Three-dimensional preliminary results of the MOOD method:
A Very High-Order Finite Volume method for Conservation Laws.

S. Diot [b,⋆], S. Clain [a,b], R. Loubère [b]

[a] Departamento de Matemática e Aplicações e Centro de Matemática, Campus de Gualtar - 4710-057 Braga, Portugal.
[b] Institut de Mathématiques de Toulouse, Université de Toulouse 31062 Toulouse, France.

[⋆] Corresponding author: steven.diot@math.univ-toulouse.fr

Abstract. *The Multi-dimensional Optimal Order Detection (MOOD) method has been designed by authors in [5] and extended in [7] to reach Very-High-Order of accuracy for systems of Conservation Laws in a Finite Volume (FV) framework on 2D unstructured meshes. In this paper we focus on the extension of this method to 3D unstructured meshes. We present preliminary results for the three-dimensional advection equation which confirm the good behaviour of the MOOD method. More precisely, we show that the scheme yields up to sixth-order accuracy on smooth solutions while preventing oscillations from appearing on discontinuous profiles.*

Keywords: MOOD; 3D; high-order; finite volume; hexahedral mesh; tetrahedral mesh; advection.

1 Introduction

The Multi-dimensional Optimal Order Detection (MOOD) has been introduced in [5–7] as an original High-Order Finite Volume method for conservation laws on 2D structured or unstructured meshes. The MOOD method is based on a high-order space discretization with local polynomial reconstructions coupled with a high-order TVD Runge–Kutta method for time discretization as any multi-dimensional MUSCL [2–4, 12] or ENO/WENO methods [1, 10, 14].

The main difference between classical high-order methods and the MOOD one is that the limitation process is done *a posteriori*. Inside a time step, a solution is first computed with numerical fluxes evaluated from unlimited high-order polynomial reconstructions. Then polynomial degrees are reduced on cells where prescribed stability or physical constraints (maximum principle, positivity, etc.) are not fulfilled. The solution is re-evaluated on these cells and their closest neighbors only. This iterative procedure converges towards a solution which respects the user-prescribed constraints.

In a previous article [7] we have shown that the MOOD method is performing well for two-dimensional geometries and can reach up to sixth-order spatial accuracy on polygonal meshes. Moreover genuinely physical problems can be simulated with the MOOD method as shown in [6, 7].

The goal of this work is to develop the 3D extension of the MOOD method with the so-called $u2$ detection process on advection problem. The paper is organized as follows. We recall the framework in section 2 and the main concepts of the MOOD method (cell/face polynomial degrees, detection process) in section 3. Then in section 4 numerical tests are carried out to show that the 3D extension of the $u2$ detection process behaves as the 2D version: Optimal rates of convergence up to sixth-order on smooth profiles and oscillation-free solutions on discontinuous profiles.

2 Framework

We consider a generic autonomous hyperbolic equation defined on a domain $\Omega \subset \mathbb{R}^3$, $t > 0$ which casts in the following conservative form

$$\partial_t U + \nabla \cdot F(U) = 0, \tag{1a}$$

$$U(\cdot, 0) = U_0, \tag{1b}$$

where $U = U(\mathbf{x}, t)$ is the vector of unknown functions, $\mathbf{x} = (x, y, z)$ denotes a point of Ω, t is the time, F is the physical flux function and U_0 is the initial condition.

The computational domain Ω is a polyhedral bounded set of $\mathbb{R}^3$ divided into convex polyhedral cells K_i, $i \in \mathcal{E}_{el}$, $\mathbf{c}_i$ being the cell centroid and $\mathcal{E}_{el}$ the cell index set. For each boundary face, $K_i \cap \partial\Omega$, we introduce a ghost cell K_j with $j \notin \mathcal{E}_{el}$ which represents the exterior side of Ω. We denote by $\mathcal{E}_{bd}$ the index set of ghost cells. $\widetilde{\mathcal{E}_{el}} = \mathcal{E}_{el} \cup \mathcal{E}_{bd}$ is the index set of cells in Ω.

For each cell K_i, one denotes by f_{ij} the common face between K_i and K_j, with $j \in \underline{\nu}(i) \subset \widetilde{\mathcal{E}_{el}}$, $\underline{\nu}(i)$ being the index set of all the elements which share a face with K_i. We assume that the mesh is built in such a way that each face is a convex polygonal. In other words any location computed as a convex combination of the points of the face lies on the face. The extended neighborhood is represented by the index set $\overline{\nu}(i) \subset \widetilde{\mathcal{E}_{el}}$ of all K_j such that $K_i \cap K_j \neq \emptyset$.

Moreover $|K_i|$ and $|f_{ij}|$ measure the volume of K_i and the surface of f_{ij} respectively while $\mathbf{n}_{ij}$ is the unit outward normal vector to f_{ij} pointing from K_i to K_j. The face being coplanar by assumption there is no ambiguity on its definition. At last, q_{ij}^r, $r = 1, ..., R$ represent the Gaussian quadrature points employed for numerical integration on a triangulation of the polygonal face f_{ij} (see Fig.1).
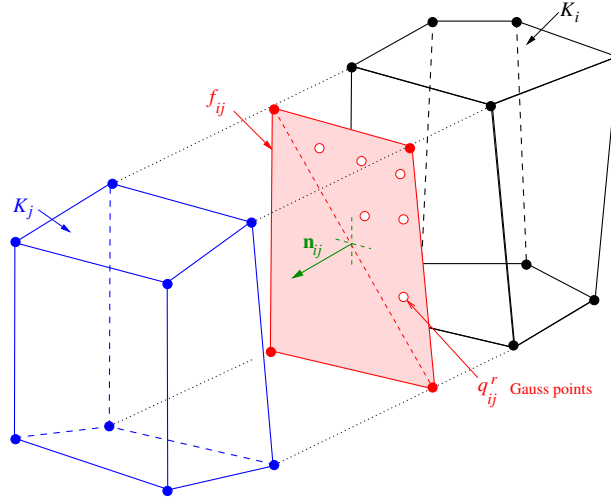

Figure 1: Mesh notation. Two neighbor cells K_i and K_j share a common face f_{ij}. $\mathbf{n}_{ij}$ is the unit outward normal vector to f_{ij} pointing from K_i to K_j. q_{ij}^r, $r = 1, ..., R$ represent the Gaussian quadrature points employed for numerical integration on face f_{ij} after triangulation.

The generic first-order explicit finite volume scheme writes as

$$U_i^{n+1} = U_i^n - \Delta t \sum_{j \in \underline{\nu}(i)} \frac{|f_{ij}|}{|K_i|} \mathbb{F}(U_i^n, U_j^n, \mathbf{n}_{ij}), \tag{2}$$

where $\mathbb{F}(U_i^n, U_j^n, \mathbf{n}_{ij})$ is a numerical consistent and monotone flux. To reach higher-order accuracy, we substitute in equation (2), the first-order approximation U_i^n and U_j^n for a better approximations of U at the quadrature points of face f_{ij}. This leads to the generic spatial high-order finite volume scheme

$$U_i^{n+1} = U_i^n - \Delta t \sum_{j \in \underline{\nu}(i)} \frac{|f_{ij}|}{|K_i|} \sum_{r=1}^{R} \xi_r \mathbb{F}(U_{ij,r}^n, U_{ji,r}^n, \mathbf{n}_{ij}), \tag{3}$$

where $U_{ij,r}^n$ and $U_{ji,r}^n$, $r = 1, ..., R$ are high-order approximations of U at quadrature points $q_{ij}^r \in f_{ij}$, $r = 1, ..., R$ respectively on both sides of face f_{ij}. The quadrature weights are denoted by ξ_r.

Let us write the scheme under the more compact form

$$U_h^{n+1} = U_h^n + \Delta t \, \mathcal{H}^R(U_h^n), \tag{4}$$

with $U_h^n = \sum\limits_{i \in \mathcal{E}_{el}} U_i^n \mathbb{1}_{K_i}$ the constant piecewise approximation of function U and operator $\mathcal{H}^R$ being defined as

$$\mathcal{H}^R(U_h^n) := - \sum_{i \in \mathcal{E}_{el}} \left(\sum_{j \in \underline{\nu}(i)} \frac{|f_{ij}|}{|K_i|} \sum_{r=1}^R \xi_r \mathbb{F}(U_{ij,r}^n, U_{ji,r}^n, \mathbf{n}_{ij}) \right) \mathbb{1}_{K_i}. \tag{5}$$

Finally a high-order method in time is provided by means of the third-order TVD Runge-Kutta method (RK3). Note that this corresponds to a convex combination of three explicit steps as follows

$$U_h^{n+1} = \frac{U_h^n + 2U_h^{(3)}}{3} \quad \text{with} \quad \left\{ \begin{array}{rcl} U_h^{(1)} & = & U_h^n + \Delta t\, \mathcal{H}^R(U_h^n) \\ U_h^{(2)} & = & U_h^{(1)} + \Delta t\, \mathcal{H}^R(U_h^{(1)}) \\ U_h^{(3)} & = & \widehat{U}_h^{(2)} + \Delta t\, \mathcal{H}^R(\widehat{U}_h^{(2)}) \end{array} \right. \tag{6}$$

where $\widehat{U}_h^{(2)}$ is the convex combination $(3U_h^n + U_h^{(2)})/4$. Note also that a high-order scheme in space and time can be rewritten as convex combinations of the first-order scheme. From a practical point of view, implementation of the high-order scheme from an initial first-order scheme is then straightforward.

3   MOOD method

For the sake of clarity, we only consider a forward Euler method and one quadrature point per face. Consequently we denote by U_{ij} (resp. U_{ji}) the high-order approximation of U on face f_{ij} from cell K_i (resp. K_j).

3.1   Basics

Polynomial reconstruction.

High-order approximations of the solution at quadrature points are constructed using multi-dimensional polynomial reconstructions from mean values. We have chosen to use the one from [10] where a over-determined linear system is solved using a QR decomposition. The reconstructed polynomial of arbitrary degree d_{max} writes

$$\widetilde{U}(x,y,z;d_{max}) = \bar{U} + \sum_{1 \leq \alpha+\beta+\gamma \leq d_{max}} \mathcal{R}_{\alpha\beta\gamma} \left((x-c_x)^\alpha (y-c_y)^\beta (z-c_z)^\gamma - \frac{1}{|K|} \int_K (x-c_x)^\alpha (y-c_y)^\beta (z-c_z)^\gamma \, dxdydz \right),$$

where (c_x, c_y, c_z) is the centroid of a generic cell K and $\mathcal{R}_{\alpha\beta\gamma}$ are the unknowns polynomial coefficients. Note that the mean value on K is conserved and the truncation of all terms of degree $\alpha + \beta + \gamma > \bar{d}$ still produces a relevant approximation of U as a polynomial of degree $\bar{d} \leq d_{max}$.

At least $\mathcal{N}(d) = (d+1)(d+2)(d+3)/6 - 1$ neighbors are needed to perform reconstructions but for the sake of robustness at least $1.5 \times \mathcal{N}(d)$ elements are involved in practice. We first take the neighbors by nodes of K plus the neighbors by faces of already chosen elements. Lastly, since the condition number of the generated system is dependent of spatial characteristic length, we use the technique proposed in [8] to overcome this problem.

CellPD, FacePD and the set of constraints $\mathcal{A}$.

We recall the fundamental notions introduced in 2D in [5, 7], here extended to 3D.

- d_i is the Cell Polynomial Degree (CellPD) which represents the degree of the polynomial reconstruction of the solution within cell K_i.

- d_{ij} and d_{ji} are the Face Polynomial Degrees (FacePD) which correspond to the actual degrees used to respectively build U_{ij} and U_{ji} on both sides of face f_{ij}.

- $\mathcal{A}$ is a set of prescribed physical and/or stability constraints. If for each cell K_i the mean values of the numerical solution fulfill the constraints then the numerical solution is said to be $\mathcal{A}$-eligible.

In this work we only focus on 3D advection problem, consequently we detail the MOOD method using both the previous notions in the case of the scalar problem.

Detection process and polynomial decrementing.

The MOOD method consists in computing a candidate solution for time t^{n+1} using the polynomial reconstructions to evaluate the fluxes. The detecting process is designed to distinguish if the candidate solution is $\mathcal{A}$-eligible. In practice we decrement the CellPD d_i of any cell K_i which does not respect all constraints of set $\mathcal{A}$. Such a cell is called *problematic*. Moreover since neighbor cells fluxes may be affected by this process, the CellPD decrementing is spread over the direct neighborhood. Once all CellPD of problematic cells have been decremented, a new candidate solution is evaluated. This decrementing procedure is repeated after each evaluation of a candidate solution up to a $\mathsf{d}_i > 0$ for which the set of constraints is fulfilled or to $\mathsf{d}_i = 0$. At that ultimate step the robust and diffusive first-order scheme is employed and its first-order solution is always taken as valid. In other words unlike traditional high-order schemes (using *a priori* limiting process), we use an *a posteriori* detecting process where the decision to alter the polynomial degree is taken after computing the candidate solution.

Solutions of autonomous scalar hyperbolic problems satisfy the Maximum Principle property. Such a property is also valid for advection problem with divergence free velocity. Therefore the Discrete Maximum Principle (DMP) seems to be a good candidate to detect problematic cells. Unfortunately the strict DMP applied to mean values drastically reduces the order of accuracy to two, and can not be used alone. Deeper studies show that the accuracy discrepancy only occurs at extrema [9, 11, 13]. We have then mainly focused on extrema since the DMP detection process is still relevant where the solution is locally monotone. We proposed in [7] a relaxation of the strict DMP at smooth extrema, called the $u2$ detection criterion, in order to avoid accuracy discrepancy that is . This leads to the introduction of an additional step into the Detection Process to reveal smooth extrema.
Therefore the first detection criteria is the DMP: No polynomial degree decrementing is performed for cells where the DMP is satisfied. Let us now consider a cell K_i where the candidate solution $U_i^\star$ does not fulfill the DMP. Two situations may arise whether we deal with a discontinuity or a smooth extrema. In [7] we have proposed a definition for the concept of a *smooth extrema* from a numerical point of view based on the following definitions.

Definition 1. Let K_i be a cell and $\widetilde{U}_i = \widetilde{U}_i(.;2)$ a polynomial reconstruction of degree 2 for an underlying function U on this cell. We define the second derivatives in x, y and z directions by $\mathcal{X}_i = \partial_{xx}\widetilde{U}_i \in \mathbb{R}$, $\mathcal{Y}_i = \partial_{yy}\widetilde{U}_i \in \mathbb{R}$ and $\mathcal{Z}_i = \partial_{zz}\widetilde{U}_i \in \mathbb{R}$. We will refer to these second derivatives as "curvatures". $\square$

For all cell K_j, $j \in \underline{\nu}(i)$, we define the maximal and minimal local curvatures as

$$\mathcal{X}_i^{min} = \min_{j\in\underline{\nu}(i)}\left(\mathcal{X}_i, \mathcal{X}_j\right) \ \text{ and } \ \mathcal{X}_i^{max} = \max_{j\in\underline{\nu}(i)}\left(\mathcal{X}_i, \mathcal{X}_j\right),$$

$$\mathcal{Y}_i^{min} = \min_{j\in\underline{\nu}(i)}\left(\mathcal{Y}_i, \mathcal{Y}_j\right) \ \text{ and } \ \mathcal{Y}_i^{max} = \max_{j\in\underline{\nu}(i)}\left(\mathcal{Y}_i, \mathcal{Y}_j\right),$$

$$\mathcal{Z}_i^{min} = \min_{j\in\underline{\nu}(i)}\left(\mathcal{Z}_i, \mathcal{Z}_j\right) \ \text{ and } \ \mathcal{Z}_i^{max} = \max_{j\in\underline{\nu}(i)}\left(\mathcal{Z}_i, \mathcal{Z}_j\right).$$

We now introduce the new detection criterion to select smooth extrema.

Definition 2. A numerical solution $U_i^\star$ in cell K_i which violates the DMP is nonetheless eligible if

$$\mathcal{X}_i^{max}\mathcal{X}_i^{min} > 0 \ \text{ and } \ \mathcal{Y}_i^{max}\mathcal{Y}_i^{min} > 0 \ \text{ and } \ \mathcal{Z}_i^{max}\mathcal{Z}_i^{min} > 0, \tag{7}$$

$$\frac{|\mathcal{X}_i^{min}|}{|\mathcal{X}_i^{max}|} \geq 1 - \varepsilon_i \ \text{ and } \ \frac{|\mathcal{Y}_i^{min}|}{|\mathcal{Y}_i^{max}|} \geq 1 - \varepsilon_i \ \text{ and } \ \frac{|\mathcal{Z}_i^{min}|}{|\mathcal{Z}_i^{max}|} \geq 1 - \varepsilon_i, \tag{8}$$

where ε_i is a cell dependent parameter defined by

$$\varepsilon_i = (\Delta x_i)^{\frac{1}{2m}}, \ \text{ with } \ \Delta x_i = |K_i|^{\frac{1}{m}}, \tag{9}$$

with m the spatial dimension, 3 in this paper. $\square$

We refer the reader to [7] for a deeper discussion and justification of such a detection process. We remark that at the limit $\varepsilon_i = 0$ we recover the DMP. In [7] we have conjectured the form of ε_i and showed that the 2D results obtained with this parameter behave as expected. Equation (9) above is its direct extension to 3D and we will show in the

numerical section that such a definition is still relevant in 3D.

Finally the MOOD method algorithm consists of the following iterative procedure.

---

1. **CellPD initialization.** Each CellPD is initialized with d_{max}.

2. **FacePD evaluation.** Each FacePD is set up as the minimum of the two neighboring CellPD.

3. **Quadrature points evaluation.** Each U_{ij} is evaluated with the polynomial reconstruction of degree d_{ij}.

4. **Mean values update.** The updated values $U_h^\star$ are computed using the finite volume scheme (3).

5. $u2$ **detection test.**

   1. The DMP criterion is first checked on each cell K_i

   $$\min_{j \in \overline{\nu}(i)} (U_i^n, U_j^n) \leq U_i^\star \leq \max_{j \in \overline{\nu}(i)} (U_i^n, U_j^n). \tag{10}$$

   2. If $U_i^\star$ does not satisfy (10) then

      a- Compute $\mathcal{X}_k, \mathcal{Y}_k, \mathcal{Z}_k$ for $k \in \underline{\nu}(i) \bigcup \{i\}$ and coefficient ε_i,

      b- Check criteria (7) and (8). If cell i is not a smooth extrema then d_i is decremented, else $U_i^\star$ is eligible.

6. **Stopping criterion.** If all cells pass the $u2$ detection test then the iterative procedure stops with $U_h^{n+1} = U_h^\star$ else go to Step 2.

Since only problematic cells and their neighbors in the compact stencil $\underline{\nu}(i)$ have to be checked and re-updated during the iterative MOOD procedure, the computational cost is dramatically reduced. Moreover the choice of reconstruction stencil is fixed at the beginning of the computation. This avoids the reconstruction of many polynomials per cell per time step and the selection of the most appropriate ones, which is in 3D a point of crucial importance.

4 Numerical results

In this work we only consider the advection equation with $F(U) = VU$ where V is the velocity $V = (u, v, w)$ on the unit cube $\Omega = [0; 1]^3$ with periodic boundary conditions. We use two types of meshes: The first one is constituted of N^3 cubes/hexahedron of size $\Delta x = \Delta y = \Delta z = 1/N$. The second one is made of $24 \times N^3$ regular tetrahedron. It is built by adding the cube center as a new vertex and further splitting each hexahedron into 24 tetrahedron, each of them sharing the cell center, see Fig.2. The goal of these tests is to show that for the two schemes MOOD-$\mathbb{P}_3$ and MOOD-$\mathbb{P}_5$ with the $u2$ detection process

- the optimal order of accuracy is reached when a smooth function is advected,

- an oscillation-free accurate solution is obtained when a discontinuous profile is advected.

As in [7] the decrementing procedure is done as follows, first from d_{max} to 2 then from 2 to 0 if necessary. Only the MOOD-$\mathbb{P}_3$ and MOOD-$\mathbb{P}_5$ schemes will be tested for the sake of brevity and conciseness.

4.1 3D convergence test

Let us consider the 3D initial sine function

$$U_0(x, y, z) = \sin(2\pi x) \sin(2\pi y) \sin(2\pi z), \tag{11}$$

and the following refined hexaedral meshes $N = 8, 16, 32, 64$ and tetrahedral meshes $N = 2, 4, 8, 16$. The advection velocity is $(1, 1, 1)$. Consequently at final time $t = 2$ the sine function is back to its initial position. The time step is taken sufficiently small to maintain the time discretization error below the spacial discretization error. In Table 1 we report the L_1, L_∞ errors and rates of accuracy for the MOOD-$\mathbb{P}_3$ and MOOD-$\mathbb{P}_5$ schemes on the two types of meshes.
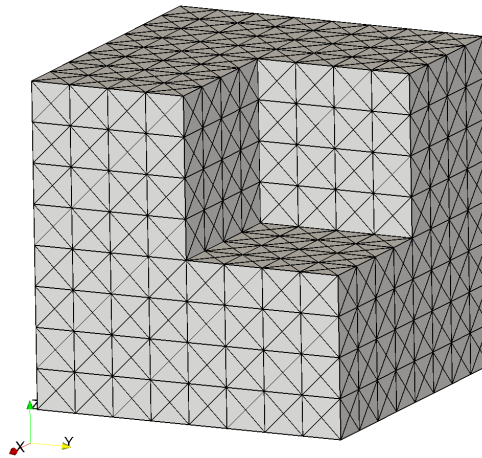
Figure 2: 24×8^2 tetrahedral mesh used for the test cases where $1/8th$ of the cube has been removed.

	Mesh	MOOD-$\mathbb{P}_3$				MOOD-$\mathbb{P}_5$			
		L_1	Rate	L_∞	Rate	L_1	Rate	L_∞	Rate
Hexahedron	8^3	$5.601e-1$	—	$6.007e-1$	—	$1.884e-1$	—	$2.034e-1$	—
	16^3	$3.557e-2$	3.98	$3.985e-2$	3.91	$2.816e-3$	6.06	$2.790e-3$	6.19
	32^3	$1.609e-3$	4.47	$2.109e-3$	4.24	$4.208e-5$	6.06	$4.040e-5$	6.11
	64^3	$8.464e-5$	4.25	$1.213e-4$	4.12	$7.794e-7$	5.75	$6.731e-7$	5.90
Tetrahedron	$2^3 \times 24$	$9.994e-1$	—	$1.046e-0$	—	$6.614e-1$	—	$8.767e-1$	—
	$4^3 \times 24$	$2.273e-1$	2.13	$2.551e-1$	2.03	$3.326e-2$	4.31	$3.366e-2$	4.70
	$8^3 \times 24$	$1.665e-2$	3.77	$1.418e-2$	4.17	$6.415e-4$	5.70	$5.029e-4$	6.06
	$16^3 \times 24$	$1.081e-3$	3.95	$8.192e-4$	4.11	$1.234e-5$	5.70	$1.038e-5$	5.59
	exact		4		4		6		6

Table 1: Errors and rates of accuracy for the advection of the sine function. MOOD-$\mathbb{P}_3$ and MOOD-$\mathbb{P}_5$ schemes. Top lines: Hexahedral mesh results — Bottom lines: Tetrahedral mesh results.

First of all one observes that the optimal order of convergence is achieved for both types of meshes. There is a genuine gain when using a $\mathbb{P}_5$ scheme, as instance the L_1 error for the 32^3 mesh is two times smaller than the $\mathbb{P}_3$ error for the 64^3 mesh. Note that the number of cells is eight times smaller and the total CPU cost for the $\mathbb{P}_5$ scheme is 6 times less expensive than for the $\mathbb{P}_3$ scheme while the memory requirement is also less important, 3.5Gb *vs* 1.6Gb. Let us remark that for this smooth profile there is no problematic cell therefore the MOOD scheme is strictly equivalent to the unlimited one (CPU time and errors). The same conclusion holds for the tetrahedral mesh.

4.2 3D Solid Body Rotation

In this section we consider the rotation of an H-like shape depicted in Fig.3-left. The computational domain is the unit cube $\Omega = [0;1]^3$ and the rotation axis is the line joining the origin and the point $(1, 1, 1)$. After one full rotation the body is back to its original position. Note that the problem is not autonomous since the velocity depends on the spatial position. Nevertheless the velocity is divergence-free leading to a divergence-free flux *i.e.* $\nabla.F(x;U) = 0$ for any constant $U \in \mathbb{R}$ so the maximum principle applies in that case.

In Fig.4 we display the results on the plane $z = 1/2$ depicted in Fig.3-right for the 40^3 hexahedron mesh for the five following schemes: MUSCL, unlimited $\mathbb{P}_3$ and $\mathbb{P}_5$ and MOOD-$\mathbb{P}_3$ and $\mathbb{P}_5$. The top views present 3D elevations while the bottom panels display the associated isolines (20 isolines between 0 (blue) and 1 (red)). Note that MUSCL
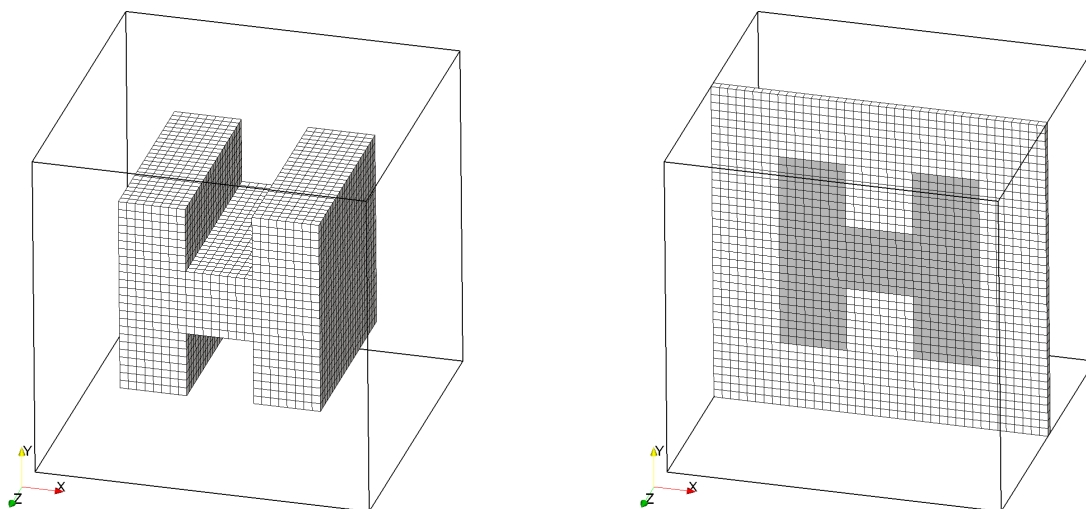
Figure 3: Solid Body Rotation test case — Left: Initialization of the body in the unit cube. We display cells with solution equals to 1 and hide the 0 valued cells — Right: Solution on the plane $z = 1/2$ (shaded cells correspond to value 1 whereas white cells to value 0).

results have been added in order to compare MOOD with this classical scheme.

We observe that the unlimited $\mathbb{P}_3$ and $\mathbb{P}_5$ schemes produce important over- and undershoots in the vicinity of the discontinuities. These oscillations could generate unphysical numerical results when real physics model is solved. Contrarily the MOOD-$\mathbb{P}_3$ and $\mathbb{P}_5$ schemes do not produce such oscillations and the shape of the body is better resolved while, as expected, the MOOD-$\mathbb{P}_5$ scheme is less diffusive than the $\mathbb{P}_3$ one.

Concerning the CPU time we observe that the MOOD method is two times more expensive than the unlimited corresponding scheme due to mandatory decrementing. Moreover the $\mathbb{P}_5$ schemes are also two times more expensive than the $\mathbb{P}_3$ ones.

Finally on average we observe 88% of cells updated with the maximal polynomial degree (3 or 5), 4% with degree 2 and 8% with degree 0 (*i.e.* first-order finite volume scheme).

5   Conclusion

In this paper we have presented the preliminary results of the 3D extension of the high-order MOOD method following the same framework as in [5–7]. These results tend to confirm that the MOOD method behavior is independent of the spatial dimension. In the numerical section we have provided evidences that the 3D MOOD method provides solutions up to sixth-order of accuracy on the advection of a smooth profile on hexahedral and tetrahedral meshes. We have also shown that on a discontinuous profile the diffusion of the MOOD method is less important with a higher polynomial degree ($\mathbb{P}_5$ *vs* $\mathbb{P}_3$ in this paper). Moreover independently of the order of accuracy the MOOD method prevents spurious oscillations from appearing.

These preliminary results and other on-going experiments tend to prove that the MOOD concept is efficient in 3D in terms of CPU and memory costs. The next step is the extension of the MOOD method to 3D hydrodynamics systems of equation.

REFERENCES

[1] R. Abgrall, On Essentially Non-oscillatory Schemes on Unstructured Meshes: Analysis and Implementation, J. Comput. Phys. **114** 45–58 (1994).

[2] T. J. Barth, Numerical methods for conservation laws on structured and unstructured meshes, VKI March 2003 Lectures Series.
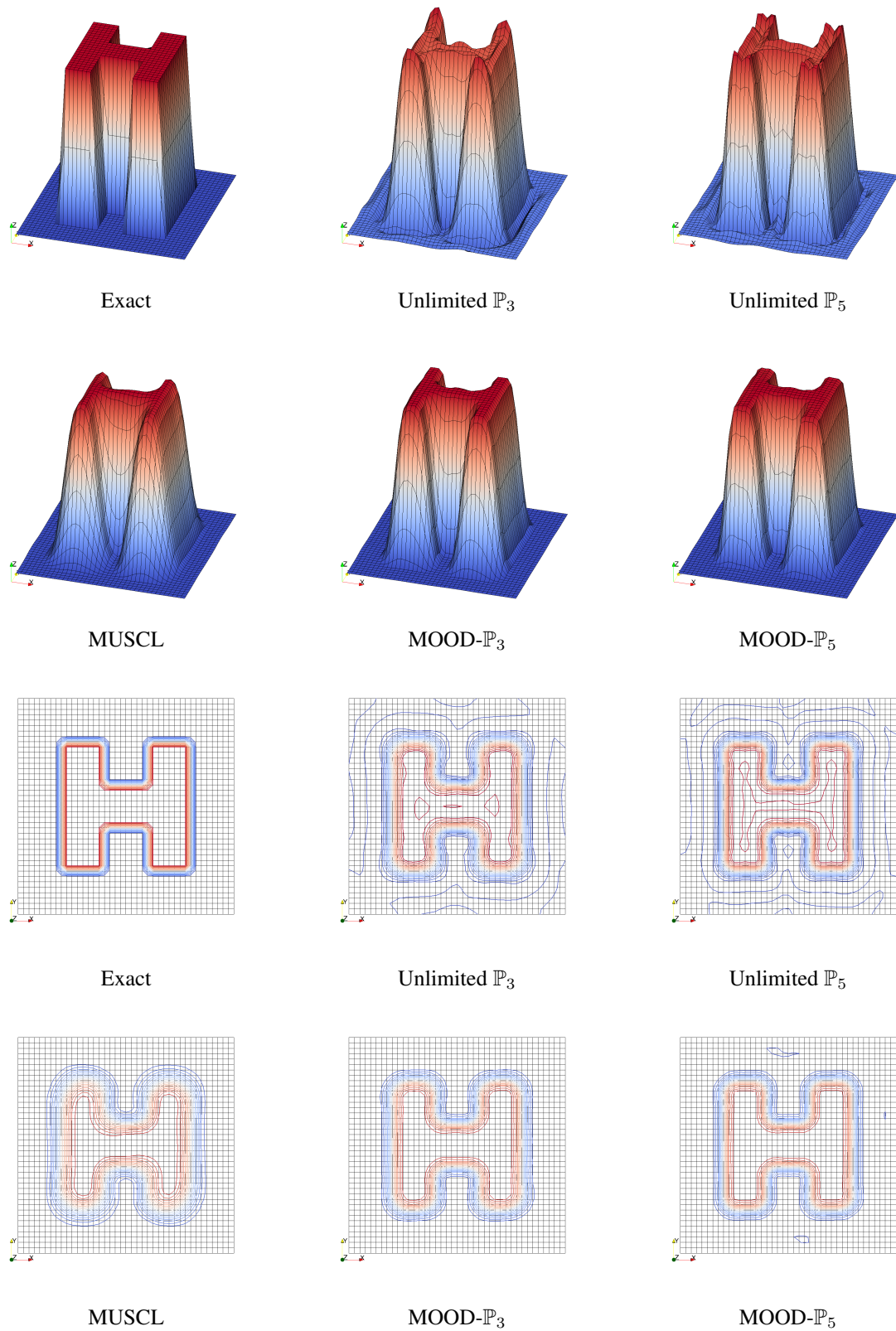
Figure 4: Solid Body Rotation test case on the 40^3 hexahedron mesh — Solution on the 2D plane $z = 1/2$ — Top: 3D elevations — Bottom: 20 isolines between 0 (blue) and 1 (red).

[3] T. J. Barth, D. C. Jespersen, The design and application of upwind schemes on unstructured meshes, AIAA Report 89-0366 (1989).

[4] T. Buffard, S. Clain, Monoslope and Multislope MUSCL Methods for unstructured meshes, J. Comput. Phys. **229** 3745-3776 (2010).

[5] S. Clain, S. Diot, R. Loubère, A high-order finite volume method for hyperbolic systems: Multi-dimensional Optimal Order Detection (MOOD), J. Comput. Phys. 230, Issue 10, pp 4028-4050, (2011).

[6] S. Clain, S. Diot, R. Loubère, Multi-dimensional Optimal Order Detection (MOOD) A very high-order Finite Volume Scheme for conservation laws on unstructured meshes, FVCA 6, International Symposium, Prague, June 6-10, 2011, Series: Springer Proceedings in Mathematics, Vol. 4, Fort, J.; Fürst, J.; Halama, J.; Herbin, R.; Hubert, F. (Eds.) 1st Edition., 2011, XVII, 1065 p. 106 illus. in color.

[7] S. Diot, S. Clain, R. Loubère, Improved detection criteria for the Multi-dimensional Optimal Order Detection (MOOD) on unstructured meshes with very high-order polynomials, in revision Comput. & Fluids (2012).

[8] O. Friedrich, Weighted Essentially Non-Oscillatory Schemes for the Interpolation of Mean Values on Unstructured Grids, J. Comput. Phys. 144 (1998) 194–212.

[9] G.-S. Jiang, E. Tadmor, Non-oscillatory central schemes for multidimensional hyperbolic conservative laws, SIAM J. Sci. Comput. 19 (1998) 1892–1917.

[10] C. F. Ollivier-Gooch, Quasi-ENO Schemes for Unstructured Meshes Based on Unlimited Data-Dependent Least-Squares Reconstruction, J. Comput. Phys. **133** 6–17 (1997).

[11] S. Osher, S. Chakravarthy, High resolution schemes and the entropy condition, SIAM J. Numer. Anal. 21 (1984) 955–984.

[12] J. S. Park, S.-H. Yoon, C. Kim, Multi-dimensional limiting process for hyperbolic conservation laws on unstructured grids, J. Comput. Phys. **229** 788–812 (2010).

[13] R. Sander, A third-order accurate variation non-expansive difference scheme for single nonlinear conservation law, Math. Comput. 51 (1988) 535–558.

[14] W. R. Wolf , J. L. F. Azevedo, High-order ENO and WENO schemes for unstructured grids, International Journal for Numerical Methods in Fluids, **55** Issue 10 917–943 (2007).